

The QGP phase in relativistic heavy-ion collisions

E. L. Bratkovskaya, V. P. Konchakovski, V. Voronyuk, V. D. Toneev, O. Linnyk,
and W. Cassing

Abstract The dynamics of partons, hadrons and strings in relativistic nucleus-nucleus collisions is analyzed within the novel Parton-Hadron-String Dynamics (PHSD) transport approach, which is based on a dynamical quasiparticle model for partons (DQPM) matched to reproduce recent lattice-QCD results - including the partonic equation of state - in thermodynamic equilibrium. The transition from partonic to hadronic degrees of freedom is described by covariant transition rates for the fusion of quark-antiquark pairs or three quarks (antiquarks), respectively, obeying flavor current-conservation, color neutrality as well as energy-momentum conservation. The PHSD approach is applied to nucleus-nucleus collisions from low SIS to RHIC energies. The traces of partonic interactions are found in particular in the elliptic flow of hadrons as well as in their transverse mass spectra.

E. L. Bratkovskaya

Institute for Theoretical Physics, University of Frankfurt, Frankfurt, Germany;
Frankfurt Institute for Advanced Study, Frankfurt am Main, Germany
e-mail: Elena.Bratkovskaya@th.physik.uni-frankfurt.de

V. P. Konchakovski

Institute for Theoretical Physics, University of Giessen, Giessen, Germany

V. Voronyuk

Bogolyubov Institute for Theoretical Physics, Kiev, Ukraine;
Joint Institute for Nuclear Research, Dubna, Russia;
Frankfurt Institute for Advanced Study, Frankfurt am Main, Germany

V. D. Toneev

Joint Institute for Nuclear Research, Dubna, Russia;
Frankfurt Institute for Advanced Study, Frankfurt am Main, Germany

O. Linnyk

Institute for Theoretical Physics, University of Giessen, Giessen, Germany

W. Cassing

Institute for Theoretical Physics, University of Giessen, Giessen, Germany

1 Introduction

The 'Big Bang' scenario implies that in the first micro-seconds of the universe the entire state has emerged from a partonic system of quarks, antiquarks and gluons – a quark-gluon plasma (QGP) – to color neutral hadronic matter consisting of interacting hadronic states (and resonances) in which the partonic degrees of freedom are confined. The nature of confinement and the dynamics of this phase transition has motivated a large community for several decades and is still an outstanding question of today's physics. Early concepts of the QGP were guided by the idea of a weakly interacting system of partons which might be described by perturbative QCD (pQCD). However, experimental observations at the Relativistic Heavy Ion Collider (RHIC) indicated that the new medium created in ultrarelativistic Au+Au collisions is interacting more strongly than hadronic matter and consequently this concept had to be severely questioned. Moreover, in line with theoretical studies in Refs. [1, 2, 3] the medium showed phenomena of an almost perfect liquid of partons [4, 5] as extracted from the strong radial expansion and the scaling of elliptic flow $v_2(p_T)$ of mesons and baryons with the number of constituent quarks and antiquarks [4].

The question about the properties of this (nonperturbative) QGP liquid is discussed controversially in the literature and dynamical concepts describing the formation of color neutral hadrons from colored partons are scarce. A fundamental issue for hadronization models is the conservation of 4-momentum as well as the entropy problem, because by fusion/coalescence of massless (or low constituent mass) partons to color neutral bound states of low invariant mass (e.g. pions) the number of degrees of freedom and thus the total entropy is reduced in the hadronization process. This problem - a violation of the second law of thermodynamics as well as the conservation of four-momentum and flavor currents - has been addressed in Ref. [6] on the basis of the DQPM employing covariant transition rates for the fusion of 'massive' quarks and antiquarks to color neutral hadronic resonances or strings. In fact, the dynamical studies for an expanding partonic fireball in Ref. [6] suggest that these problems have come to a practical solution.

A consistent dynamical approach - valid also for strongly interacting systems - can be formulated on the basis of Kadanoff-Baym (KB) equations [7] or off-shell transport equations in phase-space representation, respectively [7]. In the KB theory the field quanta are described in terms of dressed propagators with complex selfenergies. Whereas the real part of the selfenergies can be related to mean-field potentials (of Lorentz scalar, vector or tensor type), the imaginary parts provide information about the lifetime and/or reaction rates of time-like 'particles' [8]. Once the proper (complex) selfenergies of the degrees of freedom are known the time evolution of the system is fully governed by off-shell transport equations (as described in Refs. [7, 8]). The determination/extraction of complex selfenergies for the partonic degrees of freedom has been performed before in Ref. [9] by fitting lattice QCD (lQCD) 'data' within the Dynamical QuasiParticle Model (DQPM). In fact, the DQPM allows for a simple and transparent interpretation of lattice QCD results for thermodynamic quantities as well as correlators and leads to effective strongly

interacting partonic quasiparticles with broad spectral functions. For a review on off-shell transport theory and results from the DQPM in comparison to lQCD we refer the reader to Ref. [8].

The actual implementations in the PHSD transport approach have been presented in detail in Refs. [10, 11]. Here we present results for transverse mass spectra and elliptic flow of hadrons for heavy-ion collisions at relativistic energies in comparison to data from the experimental collaborations.

2 The PHSD approach

The dynamics of partons, hadrons and strings in relativistic nucleus-nucleus collisions is analyzed here within the Parton-Hadron-String Dynamics approach [6, 10, 11]. In this transport approach the partonic dynamics is based on Kadanoff-Baym equations for Green functions with self-energies from the Dynamical QuasiParticle Model (DQPM) [9] which describes QCD properties in terms of 'resummed' single-particle Green functions. In Ref. [11], the actual three DQPM parameters for the temperature-dependent effective coupling were fitted to the recent lattice QCD results of Ref. [12]. The latter lead to a critical temperature $T_c \approx 160$ MeV which corresponds to a critical energy density of $\varepsilon_c \approx 0.5$ GeV/fm³. In PHSD the parton spectral functions ρ_j ($j = q, \bar{q}, g$) are no longer δ -functions in the invariant mass squared as in conventional cascade or transport models but depend on the parton mass and width parameters:

$$\rho_j(\omega, \mathbf{p}) = \frac{\gamma_j}{E_j} \left(\frac{1}{(\omega - E_j)^2 + \gamma_j^2} - \frac{1}{(\omega + E_j)^2 + \gamma_j^2} \right) \quad (1)$$

separately for quarks/antiquarks and gluons ($j = q, \bar{q}, g$). With the convention $E^2(\mathbf{p}^2) = \mathbf{p}^2 + M_j^2 - \gamma_j^2$, the parameters M_j^2 and γ_j are directly related to the real and imaginary parts of the retarded self-energy, *e.g.* $\Pi_j = M_j^2 - 2i\gamma_j\omega$. The spectral function (1) is antisymmetric in ω and normalized as

$$\int_{-\infty}^{\infty} \frac{d\omega}{2\pi} \omega \rho_j(\omega, \mathbf{p}) = \int_0^{\infty} \frac{d\omega}{2\pi} 2\omega \rho_j(\omega, \mathbf{p}) = 1. \quad (2)$$

The actual parameters in Eq. (1), *i.e.* the gluon mass M_g and width γ_g – employed as input in the PHSD calculations – as well as the quark mass M_q and width γ_q , are depicted in Fig. 1 as a function of the scaled temperature T/T_c . As mentioned above these values for the masses and widths have been fixed by fitting the lattice QCD results from Ref. [12] in thermodynamic equilibrium.

One might worry whether the quasiparticle properties – fixed in thermal equilibrium – also should be appropriate for out-of-equilibrium configurations. This question is nontrivial and can only be answered by detailed model investigations *e.g.* on the basis of Kadanoff-Baym equations. We recall that such studies have been

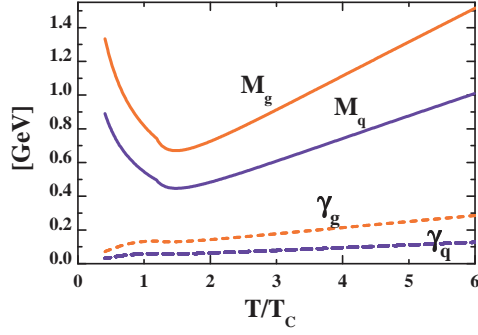


Fig. 1 The effective gluon mass M_g and width γ_g as function of the scaled temperature T/T_c (red lines). The blue lines show the corresponding quantities for quarks.

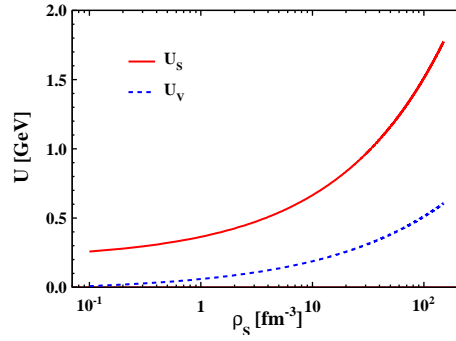


Fig. 2 The scalar and vector mean-field potentials in the present PHSD model as a function of the scalar density ρ_s of partons.

summarized in Ref. [8] for strongly interacting scalar fields that initially are far off-equilibrium and simulate momentum distributions of colliding systems at high relative momentum. The results for the effective parameters M and γ , which correspond to the time-dependent pole mass and width of the propagator, indicate that the quasiparticle properties - except for the very early off-equilibrium configuration - are close to the equilibrium mass and width even though the phase-space distribution of the particles is far from equilibrium (cf. Figs. 8 to 10 in Ref. [8]). Accordingly, we will adopt the equilibrium quasiparticle properties also for phase-space configurations out of equilibrium as appearing in relativistic heavy-ion collisions. The reader has to keep in mind that this approximation is far from being arbitrary, however, not fully equivalent to the exact solution.

We recall that the DQPM allows to extract a potential energy density V_p from the space-like part of the energy-momentum tensor which can be tabulated *e.g.* as a function of the scalar parton density ρ_s . Derivatives of V_p with respect to ρ_s then define a scalar mean-field potential $U_s(\rho_s)$ which enters the equation of motion for the dynamical partonic quasiparticles. As one can see from Fig. 2, the scalar potential is rather large and nonlinearly increases with ρ_s . This implies that the repulsive force due to $U_s(\rho_s)$ will change in a non-monotonous way with the scalar density. The vector mean-field potential is not negligible, too, especially at high ρ_s and induces a Lorentz force for the partons. Note that the vector mean-field vanishes with

decreasing scalar density whereas the scalar mean-field approaches a constant value for $\rho_s \rightarrow 0$.

Furthermore, a two-body interaction strength can be extracted from the DQPM as well from the quasiparticle width in line with Ref. [3]. The transition from partonic to hadronic d.o.f. (and vice versa) is described by covariant transition rates for the fusion of quark-antiquark pairs or three quarks (antiquarks), respectively, obeying flavor current-conservation, color neutrality as well as energy-momentum conservation [10, 11]. Since the dynamical quarks and antiquarks become very massive close to the phase transition, the formed resonant prehadronic color-dipole states ($q\bar{q}$ or qqq) are of high invariant mass, too, and sequentially decay to the groundstate meson and baryon octets increasing the total entropy.

On the hadronic side PHSD includes explicitly the baryon octet and decuplet, the 0^- - and 1^- -meson nonets as well as selected higher resonances as in the Hadron-String-Dynamics (HSD) approach [13, 14]. The color-neutral objects of higher masses (>1.5 GeV in case of baryonic states and >1.3 GeV in case of mesonic states) are treated as ‘strings’ (color-dipoles) that decay to the known (low-mass) hadrons according to the JETSET algorithm [15]. We discard an explicit recapitulation of the string formation and decay and refer the reader to the original work [15]. Note that PHSD and HSD (without explicit partonic degrees-of-freedom) merge at low energy density, in particular below the critical energy density $\epsilon_c \approx 0.5$ GeV/fm³.

The PHSD approach was applied to nucleus-nucleus collisions from $s_{NN}^{1/2} \sim 5$ to 200 GeV in Refs. [10, 11] in order to explore the space-time regions of partonic matter. It was found that even central collisions at the top-SPS energy of $\sqrt{s_{NN}} = 17.3$ GeV show a large fraction of nonpartonic, *i.e.* hadronic or string-like matter, which can be viewed as a hadronic corona [16]. This finding implies that neither hadronic nor only partonic models can be employed to extract physical conclusions in comparing model results with data.

3 Application to nucleus-nucleus collisions

In this Section we employ the PHSD approach to nucleus-nucleus collisions at moderate relativistic energies. It is of interest, how the PHSD approach compares to the HSD [14] model (without explicit partonic degrees-of-freedom) as well as to experimental data. In Fig. 3 we show the transverse mass spectra of π^- , K^+ and K^- mesons for 7% central Pb+Pb collisions at 40 and 80 A·GeV and 5% central collisions at 158 A·GeV in comparison to the data of the NA49 Collaboration [17]. Here the slope of the π^- spectra is only slightly enhanced in PHSD relative to HSD which demonstrates that the pion transverse motion shows no sizeable sensitivity to the partonic phase. However, the K^\pm transverse mass spectra are substantially hardened with respect to the HSD calculations at all bombarding energies - *i.e.* PHSD is more in line with the data - and thus suggests that partonic effects are better visible in the strangeness-degrees of freedom.

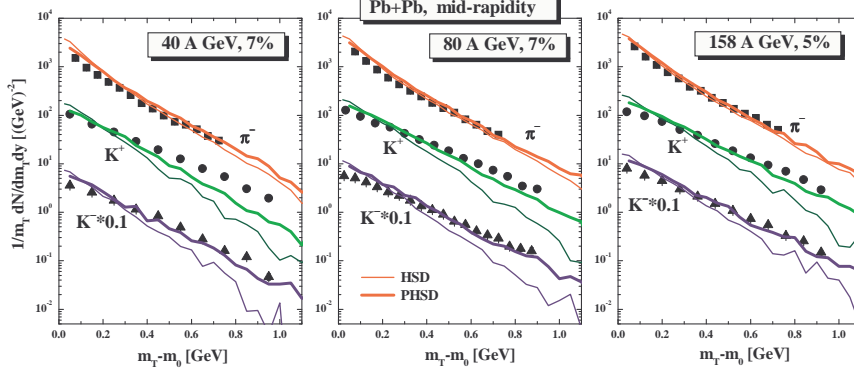


Fig. 3 The π^- , K^+ and K^- transverse mass spectra for central Pb+Pb collisions at 40, 80 and 158 A·GeV from PHSD (thick solid lines) in comparison to the distributions from HSD (thin solid lines) and the experimental data from the NA49 Collaboration [17].

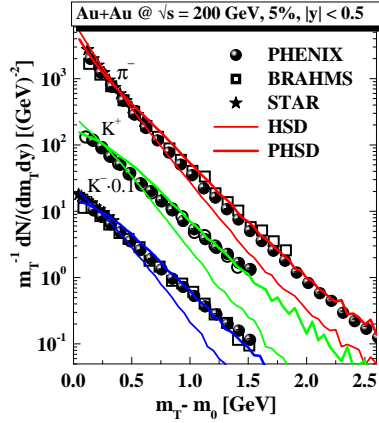


Fig. 4 The π^- , K^+ and K^- transverse mass spectra for 5% central Au+Au collisions at $\sqrt{s} = 200$ GeV from PHSD (thick solid lines) in comparison to the distributions from HSD (thin solid lines) and the experimental data from the BRAHMS, PHENIX and STAR Collaborations [18, 19, 20] at midrapidity.

The PHSD calculations for RHIC energies show a very similar trend - the inverse slope increases by including the partonic phase - cf. Fig. 4 where we show the transverse mass spectra of π^- , K^+ and K^- mesons for 5% central Au+Au collisions at $\sqrt{s} = 200$ GeV in comparison to the data of the RHIC Collaborations [18, 19, 20].

The hardening of the kaon spectra can be traced back to parton-parton scattering as well as a larger collective acceleration of the partons in the transverse direction due to the presence of repulsive vector fields for the partons. The enhancement of the spectral slope for kaons and antikaons in PHSD due to collective partonic flow shows up much clearer for the kaons due to their significantly larger mass (relative to pions). We recall that in Refs. [21] the underestimation of the K^\pm slope by HSD (and also UrQMD) had been suggested to be a signature for missing partonic degrees of freedom; the present PHSD calculations support this early suggestion.

The strange antibaryon sector is of further interest since here the HSD calculations have always underestimated the yield [22]. Our detailed studies in Ref. [10]

show that the HSD and PHSD calculations both give a reasonable description of the $\Lambda + \Sigma^0$ yield of the NA49 Collaboration [23]; both models underestimate the NA57 data [24] by about 30%. An even larger discrepancy in the data from the NA49 and NA57 Collaborations is seen for $(\bar{\Lambda} + \bar{\Sigma}^0)/N_{wound}$; here the PHSD calculations give results which are in between the NA49 data and the NA57 data whereas HSD underestimates the $(\bar{\Lambda} + \bar{\Sigma}^0)$ midrapidity yield at all centralities.

The latter result suggests that the partonic phase does not show up explicitly in an enhanced production of strangeness (or in particular strange mesons and baryons) but leads to a different redistribution of antistrange quarks between mesons and antibaryons. In fact, as demonstrated in Ref. [10], we find no sizeable differences in the double strange baryons from HSD and PHSD – in a good agreement with the NA49 data – but observe a large enhancement in the double strange antibaryons for PHSD relative to HSD.

The anisotropy in the azimuthal angle ψ is usually characterized by the even order Fourier coefficients $v_n = \langle \exp(in(\psi - \Psi_{RP})) \rangle$, $n = 2, 4, \dots$, since for a smooth angular profile the odd harmonics become equal to zero. As noted above, Ψ_{RP} is the azimuth of the reaction plane and the brackets denote averaging over particles and events. In particular, for the widely used second order coefficient, denoted as an elliptic flow, we have

$$v_2 = \langle \cos(2\psi - 2\Psi_{RP}) \rangle = \left\langle \frac{p_x^2 - p_y^2}{p_x^2 + p_y^2} \right\rangle, \quad (3)$$

where p_x and p_y are the x and y components of the particle momenta. This coefficient can be considered as a function of centrality, pseudo-rapidity η and/or transverse momentum p_T . We note that the reaction plane in PHSD is given by the $(x - z)$ plane with the z -axis in the beam direction.

In Fig. 5 the experimental v_2 excitation function in the transient energy range is compared to the results from the PHSD calculations [30]; HSD model results are given as well for reference. We note that the centrality selection and acceptance are the same for the data and models.

We recall that the HSD model has been very successful in describing heavy-ion spectra and rapidity distributions from SIS to SPS energies. A detailed comparison of HSD results with respect to a large experimental data set was reported in Refs. [27, 21, 28] for central Au+Au (Pb+Pb) collisions from SIS to top SPS energies. Indeed, as shown in Fig. 5 (dashed lines), HSD is in good agreement with experiment for both data sets at the lower edge ($\sqrt{s_{NN}} \sim 10$ GeV) but predicts an approximately energy-independent flow v_2 at larger energies and, therefore, does not match the experimental observations. This behavior is in quite close agreement with another independent hadronic model, the UrQMD (Ultra relativistic Quantum Molecular Dynamics) [29] (cf. with Ref. [25]).

From the above comparison one may conclude that the rise of v_2 with bombarding energy is not due to hadronic interactions and models with partonic d.o.f. have to be addressed. Indeed, the PHSD approach incorporates the parton medium ef-

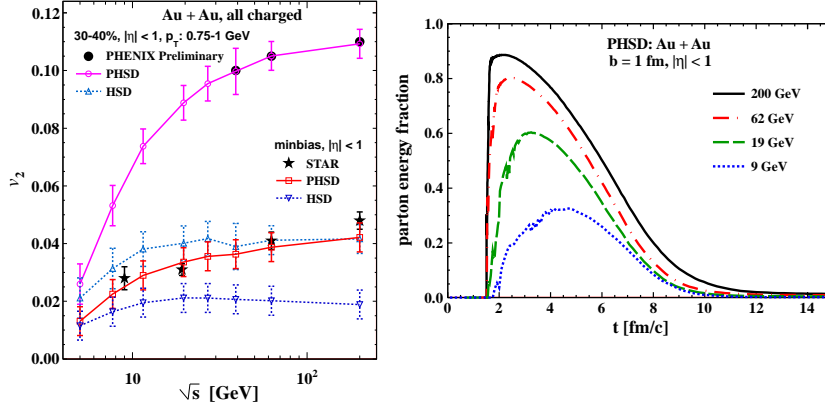


Fig. 5 (Left:) Average elliptic flow v_2 of charged particles at midrapidity for two centrality selections calculated within the PHSD (solid curves) and HSD (dashed curves). The v_2 STAR data compilation for minimal bias collisions are taken from [25] (stars) and the preliminary PHENIX data [26] are plotted by filled circles.

Fig. 6 (Right:) The evolution of the parton fraction of the total energy density at mid-pseudorapidity for different collision energies.

fects in line with a IQCD equation-of-state, as discussed above, and also includes a dynamic hadronization scheme based on covariant transition rates. It is seen from Fig. 5 that PHSD performs better: The elliptic flow v_2 from PHSD (solid curve) is fairly in line with the data from the STAR and PHENIX collaborations and clearly shows the growth of v_2 with the bombarding energy [30].

The v_2 increase is clarified in Fig. 6 where the partonic fraction of the energy density at mid-pseudorapidity with respect to the total energy density in the same pseudorapidity interval is shown. We recall that the repulsive scalar mean-field potential $U_s(\rho_s)$ for partons in the PHSD model leads to an increase of the flow v_2 as compared to that for HSD or PHSD calculations without partonic mean fields. As follows from Fig. 6, the energy fraction of the partons substantially grows with increasing bombarding energy while the duration of the partonic phase is roughly the same.

The v_2 coefficient measures the response of the heated and compressed matter to the spatial deformation in the overlap region of colliding nuclei, which is usually quantified by the eccentricity $\varepsilon_2 = \langle y^2 - x^2 \rangle / \langle x^2 + y^2 \rangle$. Since the flow response (v_2) is proportional to the driving force (ε_2), the ratio v_2/ε_2 is used to compare different impact parameters and nuclei.

A remarkable property – *universal scaling* – has been proposed in Ref. [31] (see Fig. 7). It appears that v_2/ε_2 plotted versus $(1/S)dN_{ch}/dy$ falls on a ‘universal’ curve, which links very different regimes, ranging from AGS to RHIC energies. Here $S = \pi\sqrt{\langle x^2 \rangle \langle y^2 \rangle}$ is the overlap area of the collision system and dN_{ch}/dy is the rapidity density of charged particles.

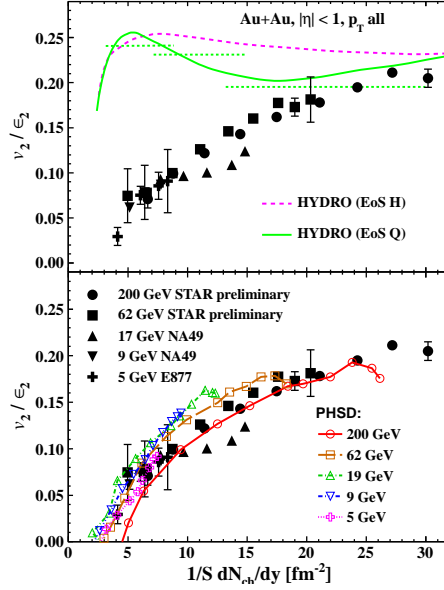


Fig. 7 Scaling of v_2/ϵ_2 vs $(1/S)(dN_{ch}/dy)$. The PHSD results [32] are given by lines with open symbols. Predictions of ideal boost-invariant hydrodynamics are shown in the top panel (from [33]) and explained in the text. Our PHSD results are presented in the bottom panel. The experimental data points for Au+Au collisions at 200 GeV (circles) and 62 GeV (squares) are from Refs. [33, 34].

As seen from Fig. 7 (lower panel) the universal scaling of v_2/ϵ_2 versus $(1/S)dN_{ch}/dy$ is approximately reproduced by PHSD (see Ref. [32] for the details). This feature is not reproduced by hadronic transport models (such as HSD and UrQMD) and meets (severe) problems in the various hydrodynamic descriptions as demonstrated in the upper panel of Fig. 7 for a pure hadronic equation of state ('EoS H') as well as with a QGP phase transition ('EoS Q').

Thus, the experimentally observed scaling in Fig. 7 puts very strong constraints on the initial microscopic properties (entropy density, mean free path, *etc.*), as well as the global longitudinal structure [35].

Work supported in part by the HIC for FAIR framework of the LOEWE program and by DFG.

References

1. E. Shuryak, Prog. Part. Nucl. Phys. 53, 273 (2004).
2. M. H. Thoma, J. Phys. G 31, L7 (2005); Nucl. Phys. A 774, 307 (2006).
3. A. Peshier and W. Cassing, Phys. Rev. Lett. 94, 172301 (2005).
4. I. Arsene *et al.*, Nucl. Phys. A 757, 1 (2005); B. B. Back *et al.*, Nucl. Phys. A 757, 28 (2005); J. Adams *et al.*, Nucl. Phys. A 757, 102 (2005); K. Adcox *et al.*, Nucl. Phys. A 757, 184 (2005).
5. T. Hirano and M. Gyulassy, Nucl. Phys. A 769, 71 (2006).
6. W. Cassing and E. L. Bratkovskaya, Phys. Rev. C 78, 034919 (2008).

7. S. Juchem, W. Cassing and C. Greiner, Phys. Rev. D 69, 025006 (2004); Nucl. Phys. A 743, 92 (2004).
8. W. Cassing, E. Phys. J. ST 168, 3 (2009).
9. W. Cassing, Nucl. Phys. A 795, 70 (2007).
10. W. Cassing and E. L. Bratkovskaya, Nucl. Phys. A 831, 215 (2009).
11. E. L. Bratkovskaya, W. Cassing, V. P. Konchakovski, O. Linnyk, Nucl. Phys. A 856, 162 (2011).
12. Y. Aoki *et al.*, JHEP 0906, 088 (2009).
13. W. Ehehalt and W. Cassing, Nucl. Phys. A 602, 449 (1996).
14. W. Cassing and E. L. Bratkovskaya, Phys. Rep. 308, 65 (1999).
15. H.-U. Bengtsson and T. Sjöstrand, Comp. Phys. Commun. 46, 43 (1987).
16. J. Aichelin and K. Werner, Phys. Rev. C 79, 064907 (2009).
17. C. Alt *et al.*, NA49 Collaboration, Phys. Rev. C 66, 054902 (2002); Phys. Rev. C 77, 024903 (2008).
18. S. S. Adler *et al.*, Phys. Rev. C 69, 034909 (2004).
19. J. Adams *et al.*, Phys. Rev. Lett. 92, 112301 (2004).
20. I. G. Bearden *et al.*, Phys. Rev. Lett. 94, 162301 (2005).
21. E. L. Bratkovskaya, S. Soff, H. Stöcker, M. van Leeuwen, and W. Cassing, Phys. Rev. Lett. 92, 032302 (2004).
22. J. Geiss, W. Cassing and C. Greiner, Nucl. Phys. A 644, 107 (1998).
23. T. Anticic *et al.*, Phys. Rev. C 80, 034906 (2009).
24. F. Antinori *et al.*, Phys. Lett. B 595, 68 (2004); J. Phys. G: Nucl. Phys. 32, 427 (2006).
25. M. Nasim, L. Kumar, P. K. Netrakanti and B. Mohanty, Phys. Rev. C **82**, 054908 (2010).
26. X. Gong *et al.*, J. Phys. G 38, 124146 (2011).
27. E. L. Bratkovskaya, W. Cassing, and U. Mosel, Phys. Lett. B 424, 244 (1998).
28. E. L. Bratkovskaya, *et al.*, Phys. Rev. C 69, 054907 (2004).
29. S. A. Bass *et al.*, Prog. Part. Nucl. Phys. 41, 255 (1998); M. Bleicher *et al.*, J. Phys. G 25, 1859 (1999).
30. V.P. Konchakovski *et al.*, Phys. Rev. C 85, 011902(R) (2012).
31. S.A. Voloshin and A.M. Poskanzer, Phys. Lett. B 474, 27 (2000).
32. V.P. Konchakovski *et al.*, arXiv:1201.3320 [nucl-th].
33. S. A. Voloshin, J. Phys. G **34**, S883 (2007).
34. M. Shimomura *et al.*, PoS WPCF2011, 070 (2011).
35. G. Torrieri, Phys. Rev. C **76**, 024903 (2007).